JOURNAL OF GUIDANCE, CONTROL, AND DYNAMICS
Vol. 20, No. 6, November–December 1997

Compensation for Distributed Hysteresis Operators in Active Structural Systems

A. J. Kurdila* and G. Webb†
Texas A&M University, College Station, Texas 77843-3141

A class of integral, hysteretic control influence operators is derived for the representation of structural systems exhibiting hysteresis due to active materials. The hysteretic control influence operator is defined in terms of a probability distribution, or more generally a measure, that describes the concentration of a particular hysteresis kernel. Specifically, two types of hysteresis kernels are studied in detail: the ideal relay kernel leading to a Preisach integral hysteresis operator and a generalized play kernel leading to a Krasnosel'skii–Pokrovskii operator. When combined with the thermal and structural dynamics equations, the governing equations are history-dependent integropartial differential equations, coupled in a cascade structure. Existence, uniqueness, and convergence of Galerkin approximation methods have been derived for the forward simulation and model identification. The cascade structure of the coupled, nonlinear partial differential equations is advantageous in that model reference control and model reference adaptive control strategies can be derived for the systems under consideration. Numerical and experimental results that validate the theoretical developments are presented.

I. Introduction

A CONFLUENCE of research efforts in materials science, micromechanics, and control theory has lead to a growing interest in the emerging class of active materials. Roughly speaking, active materials are those materials that exhibit large, nonnegligible and direct mechanical response with the application of electric or magnetic fields. Some of the most common active materials in use today include piezoceramics (PZT), shape memory alloys (SMA), electrorheological fluids (ERF), and magnetorheological fluids (MRF). In some sense, these materials have served as the prototypical examples of the class of active materials and exhibit a wide range of physical response characteristics including actuation authority and bandwidth. However, the synthesis of new classes of active materials is a growing area of research, and it is reasonable to believe that new types of hybrid materials will emerge that exhibit response characteristics that are intermediate to those of, e.g., SMA, PZT, ERF, and MRF. As a whole, these materials pose a formidable challenge to researchers interested in applying them to aerospace structures. To varying degrees, each of these materials exhibit hysteresis in their mechanical response. For example, whereas piezoceramics are often modeled as linear systems, it is well known that they can exhibit hysteresis for high electric field strengths.[1,2] The mechanical response of ERF and MRF are profoundly hysteretic. Kamath et al.[3] show that the shear modulus in ERF is not only hysteretic, the hysteresis is nonstationary in that it depends parametrically on the current. Similar phenomena have been reported for MRF, although in this case the hysteresis cycles depend parametrically on the magnetic field strength. Research that studies the modeling of the thermomechanical response of SMA[4] illustrates that hysteresis cycles are evident in measurements of strain vs temperature when actuation is induced thermally, or stress vs strain in the isothermal case.

We present recent research that is aimed at providing a systematic formulation appropriate for a class of structures that are controlled using active materials. The formulation considers those nonlinear systems in which we are able to model the active material actuation device as a nonlinear, integral hysteresis operator. We assume that the structural system to be controlled can be accurately represented via linear system theory. Hence, although the open-loop dynamical system is nonlinear, it has a cascade structure. That is, the system response is achieved by cascading a nonlinear control influence operator and a linear structural system. For this class of systems, a fairly complete theory can be developed. We summarize recent results by Banks et al.[5,6] that illustrate that the identification problem, in which we seek to determine the hysteresis operator from structural measurement, is well posed. We show that a convergent Galerkin approximation scheme can be derived for this class of coupled, nonlinear identification problems. In addition, once the hysteretic control influence operator has been identified, we discuss the existence and construct feedforward approximate inverses for the integral hysteretic control influence operators. Finally, we employ feedforward approximate inverses in model reference control (MRC) and model reference adaptive control (MRAC) schemes. Stability for the closed-loop system is proven, under suitable (conventional) model matching conditions.

The research presented in this paper draws heavily upon a large collection of papers that have appeared in print that study 1) constitutive laws for SMA, 2) the mathematical properties of hysteresis operators, 3) model reference and adaptive control, and 4) previous research that treats control using shape memory alloys. In particular, the reader may refer to several works[4,7,8] and the references therein to gain an appreciation of the complexity of constitutive laws derived for shape memory alloys. Ivshin and Pence[9] discuss a simple, effective (but phenomenological) model for hysteretic phase transition behavior in SMA, whereas Coleman and Hodgon[10,11] study similar constructions for characterizing ferromagnetic hysteresis. The subtleties involved in deriving mathematical properties of hysteresis operators is studied in the seminal work of Krasnosel'skii and Pokrovskii (KP)[12] and in the excellent monographs by Mayergoyz[13] and Visintin.[14] Surveys of the current spectrum of technical results available on hysteresis can be found in Brokate[15] and in Macki et al.[16] Inasmuch as we employ model reference and adaptive control for the closed-loop control design, the reader is referred to Ioannou and Sun[17] or Sastry and Bodson[18] for the details of several proofs outlined in the latter part of this paper. In addition, the work of Tao and Kokotovic[2,19] for piecewise linear hysteretic systems has been essential in this paper. Our results for closed-loop MRC and MRAC for classes of Preisach and KP integral operators can be viewed as straightforward applications of their work. Finally, it should be noted that a considerable number of innovative SMA actuator designs and associated heuristic control methodologies have been presented over the past few years.[20,21]

Received Nov. 10, 1996; presented as Paper 97-0361 at the AIAA 35th Aerospace Sciences Meeting, Reno, NV, Jan. 6–9, 1997; revision received May 1, 1997; accepted for publication May 16, 1997.

*Associate Professor, Department of Aerospace Engineering. Member AIAA.
†Ph.D. Candidate, Department of Aerospace Engineering. Student Member AIAA.

II. Hysteretic Operators

We will investigate dynamical systems that contain a structural subsystem that can be accurately represented by linear system theory, one that is actuated by active materials that are inherently hysteretic. More precisely, we assume that the controller's influence on the structure can be represented as an integral hysteresis operator P_μ

$$[P_\mu(u, I)](t) = \int_{S_\Delta} \{k_s[u, I(s)]\}(t)\, \mathrm{d}\mu(s)$$

In this equation, $k_s(u, \xi)$ is a particular hysteresis kernel that maps the continuous input signal u into a prototypical hysteretic response. The value ξ represents the initial condition of the kernel and $I(s)$ is a function that specifies the initial condition of the kernel for each value of s. The variable s parameterizes a family of hysteresis kernels over a set of admissible parameters S_Δ. Thus, the response of the hysteretic control influence operators is an average, or weighted sum, of responses of several fundamental hysteretic response. The term $\mu(s)$ is a probability distribution, perhaps represented by a probability density, that specifies the effective contribution of the hysteresis introduced by $k_s(u, \xi)$ for each value of s. For example, if we model the response by a finite linear combination of prototypical hysteretic responses, the overall response is given by

$$[P_\mu(u, I)](t) = \sum_{i=1}^{N} \mu_i \left\{k_{s_i}[u, I(s_i)]\right\}(t)$$

In this case, the probability distribution $\mu(s)$ is a finite sum of atoms

$$\mu(s) = \sum_{i=1}^{N} \mu_i \delta_{s_i}$$

where each ξ_{s_i} is the Dirac measure concentrated at $s_i \in S_\Delta$, $\mu_i > 0$, and

$$\sum_i \mu_i = 1$$

This example shows that the class of hysteresis operators we consider can be considered rheological; they are the finite or infinite sum of parallel hysteresis elements. We will consider two different classes of hysteretic kernels in this paper, the Preisach kernel $\tilde{k}$ and the KP kernel $\hat{k}$. Together, these two classes of hysteresis operators account for qualitatively different hysteretic response. For example, Fig. 1 shows the output of the Preisach and KP kernels for a sample input signal. Roughly speaking, the KP kernel output appears as a smoothed version of the Preisach kernel output when we consider major loop response. More significant differences are apparent when we consider minor loop response as will be discussed. To completely specify the behavior of the Preisach kernel, consider the kernel $\hat{k}_s$ shown in Fig. 1. If the input $u(t)$ increases from a level of negative saturation (equal to -1) to the switch value s_2, the output jumps to state of positive saturation $+1$. If the input $u(t)$ subsequently decreases to a level s_1, the output response jumps to a state of negative saturation. Thus, we see that each Preisach kernel is characterized by a set of two switching values $s = (s_1, s_2)$. The set of all possible switching values is denoted

$$S = \left\{s \in R^2 : s = (s_1, s_2),\, s_1 < s_2\right\}$$

and is referred to as the Preisach plane. For computational purposes, we only consider a bounded triangle S_Δ in the Preisach plane defined as

$$S_\Delta = \left\{s \in R^2 : s = (s_1, s_2),\, \underline{s} < s_1 < s_2 < \bar{s}\right\}$$

where $\underline{s}$ and $\bar{s}$ are two fixed constants. By introducing the switching times

$$\tau(t) = \{\eta \in [0, T] : u(\eta) = s_1 \quad \text{or} \quad u(\eta) = s_2\}$$

the Preisach kernel is defined to be

$$[\tilde{k}_s(u, \xi)](t) = \begin{cases} [\tilde{k}_s(u, \xi)](0) & \text{if} \quad \tau(t) = \emptyset \\ -1 & \text{if} \quad \tau(t) \neq \emptyset \quad \text{and} \quad u\{\max[\tau(t)]\} = s_1 \\ +1 & \text{if} \quad \tau(t) \neq \emptyset \quad \text{and} \quad u\{\max[\tau(t)]\} = s_2 \end{cases}$$

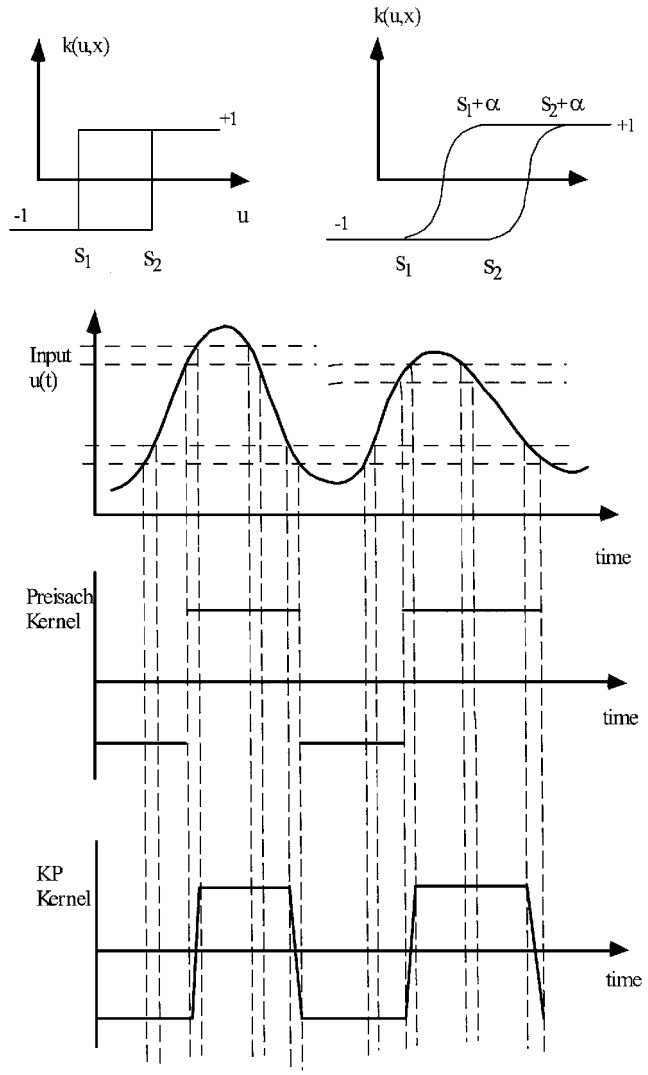

Fig. 1 Hysteresis kernels: major loop response.

The variable ξ defines the initial condition of the kernel via

$$[\tilde{k}_s(u, \xi)](0) = \begin{cases} -1 & \text{if} \quad u(0) \leq s_1 \\ \xi & \text{if} \quad s_1 < u(0) < s_2 \\ +1 & \text{if} \quad u(0) \geq s_2 \end{cases}$$

For the purposes of this paper, we will define the output of the KP hysteretic kernel for piecewise linear inputs only. The subtleties involved in deriving the KP operator for arbitrary continuous functions is beyond the scope of this paper, and the reader is referred to Refs. 12 and 14 for the details in this case. The response of the KP kernel always lies within the envelope defined by the translated ridge functions $r(x - s_1)$ and $r(x - s_2)$ shown in Fig. 1. We define the monotone output operator to be given for $\tilde{u}$ nondecreasing and for $\tilde{u}$ nonincreasing as

$$[M(\tilde{u}, \xi)](t) = \begin{cases} \max\{\xi, r[\tilde{u}(t) - s_2]\} \\ \min\{\xi, r[\tilde{u}(t) - s_1]\} \end{cases}$$

respectively, whenever $\tilde{u}$ is a monotone function and ξ is some initial condition. If u is a piecewise linear function, the KP kernel is subsequently defined via recursion. We let $\mathcal{M}_0 = \xi$ and define

$$[\hat{k}_s(u, \xi)](t) = \begin{cases} [M(u, M_{k-1})](t) & \text{for} \quad t \in [t_{k-1}, t_k] \\ M_k = M(u, M_{k-1})(t_k) & \text{for} \quad k = 1, \ldots, j \end{cases}$$

III. Governing Equations

The class of systems we will consider can be represented by the coupled system of evolution equations written in weak form as

$$\langle \ddot{w}(t), \phi \rangle_{V^* \times V} + a_1[\dot{w}(t), \phi] + a_0[w(t), \phi] = \langle \{B_\mu[M(T)]\}(t), \phi \rangle_{V^* \times V}, \qquad \forall \phi \in V \tag{1}$$

$$\langle T(t), \psi \rangle_{W^* \times W} + b_0[T(t), \psi] = \langle Bu(t), \psi \rangle_{W^* \times W}, \qquad \forall \psi \in W \tag{2}$$

We have chosen to represent the equations of motion in weak form so as to accommodate a class of structural systems including elastic rods, beams, plates, shells, and linearly elastic solids. Indeed, these equations include both finite-dimensional and infinite-dimensional dynamical systems. In general, V and W are Banach spaces in which the state variables $w(t)$, $\dot{w}(t)$, and $T(t)$ evolve, and the notation $\langle \cdot\,, \cdot \rangle_{V^* \times V}$ and $\langle \cdot\,, \cdot \rangle_{W^* \times W}$ denote the duality pairing on these spaces. The existence, uniqueness, and convergence of approximations for the infinite-dimensional structural subsystem in these equations has been discussed in previous papers.[5,6] Although we retain this notation to summarize the treatment of infinite-dimensional dynamical systems in identification problems discussed in Sec. IV, only finite-dimensional spaces are considered in the derivation of control strategies, numerical results and experimental results presented. Typically, the finite-dimensional dynamical systems are derived from Eq. (1) via Galerkin approximation, to be discussed shortly. In this case, we can interpret $\langle \cdot\,, \cdot \rangle_{V^* \times V}$ and $\langle \cdot\,, \cdot \rangle_{W^* \times W}$ as just the inner product. In these equations, $w(t)$, $\dot{w}(t)$, and $\ddot{w}(t)$ are the structural displacement, velocity, and acceleration, respectively. The temperature of the SMA actuation system is characterized by $T(t)$. The terms $a_1(\cdot\,, \cdot)$ and $a_0(\cdot\,, \cdot)$ represent the damping bilinear form and stiffness bilinear form for the structural system, whereas $b_0(\cdot\,, \cdot)$ is the bilinear form characterizing the heat equation. The input current is given by $u(t)$.

We utilize finite-dimensional approximations of the dynamical systems in Eqs. (1) and (2). We choose a finite, linearly independent basis $\{\phi_i\}_{i=1}^N \subseteq V$ and $\{\psi_i\}_{i=1}^M \subseteq W$, and approximate the unknown states via

$$w(t) = \sum_{i=1}^{N} w_i(t)\phi_i \tag{3}$$

$$T(t) = \sum_{j=1}^{M} T_j(t)\psi_j \tag{4}$$

As a result, the Galerkin approximations of the governing equations in Eqs. (1) and (2) can be written as

$$[M]\ddot{w}(t) + [C]\dot{w}(t) + [K]w(t) = [B_\mu(w)](t) \tag{5}$$

$$[N]\dot{T}(t) + [L]T(t) = [B]u(t) \tag{6}$$

where the entries of the constituent matrices are given by $M_{ij} = \langle \phi_i, \phi_j \rangle$, $C_{ij} = a_1(\phi_i, \phi_j)$, $K_{ij} = a_0(\phi_i, \phi_j)$, $L_{ij} = b_0(\psi_i, \psi_j)$, and $N_{ij} = \langle \psi_i, \psi_j \rangle$. The actual structure of the nonlinear operator depends on the physical example and on the approximation methodology. A discussion of convergent Galerkin approximations of $[B_\mu(w)](t)$ determined from $B_\mu[M(T), f]$ is discussed in Ref. 5. Conditions that guarantee that the structural part of this system of dynamical equations is well posed can be found in several places, for example, in Ref. 22. Instead of axiomatically defining properties that define the operators comprising the abstract governing equations directly, we summarize several examples of the systems modeled in Eqs. (3–6).

Example 1

In the simplest example considered (Fig. 2), we consider a system comprising a spring, mass, and damper that is suspended by an SMA wire. The equations of motion for this system can be written as

$$m\ddot{y}(t) + C\dot{y}(t) + Ky(t) = -mg + \int_{\mathcal{S}_\Delta} \{k_s[M(T), I(s)]\}(t)\, \mathrm{d}\mu(s) \tag{7}$$

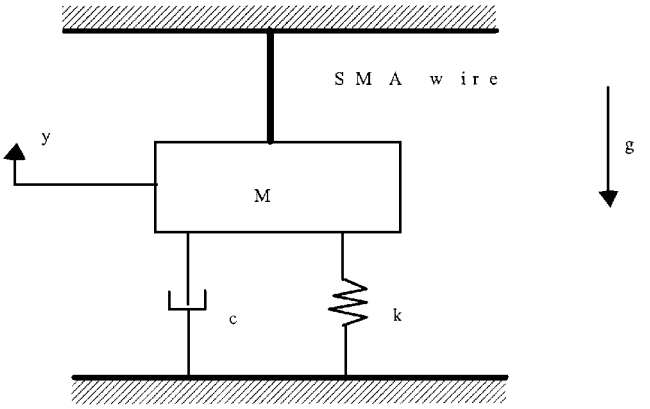

Fig. 2 Mass-damper-spring system supported by SMA wire.

$$\frac{\partial T(y,z)}{\partial t} = \kappa \nabla^2 T + \frac{1}{\rho c} Q_0, \qquad y, z \in \Omega \tag{8}$$

$$\frac{k \partial T}{\partial n} = -h(T - T_\infty), \qquad y, z \in \partial\Omega \tag{9}$$

subject to the initial conditions

$$y(0) = y_0 \tag{10}$$

$$\dot{y}(0) = y_1 \tag{11}$$

$$T(0) = T_0 \tag{12}$$

In these equations, m, C, and K are the mass, damping, and stiffness coefficients, whereas $y(t)$ is the displacement of the mass. The temperature of the thermally activated wire is $T(t)$, k is the thermal conductivity, $\kappa = k/\rho c$ is the thermal diffusivity, ρ is the mass density per unit length of the SMA wire, c is the specific heat, and Q_0 is the heat density per unit length of the SMA wire. The heat density per unit length is generated by resistive heating of the wire and is proportional to the square of the current i by the equation

$$Q_0 = (r/A)i^2 \tag{13}$$

where r is the resistivity and A is the cross-sectional area of the SMA wire.

Example 2

Our second example (Fig. 3) models a Bernoulli–Euler beam with two embedded SMA layers. If we assume that the structure exhibits proportional damping, the strong form of the governing equations can be shown to be

$$\rho \frac{\partial^2 w}{\partial t^2} + EI \frac{\partial^2}{\partial x^2}\left(\frac{\partial^2 w}{\partial x^2}\right) + c_D I \frac{\partial^2}{\partial x^2}\left(\frac{\partial^3 w}{\partial x^2 \partial t}\right) = \frac{\partial^2}{\partial x^2}\left(\int_{\mathcal{S}_\Delta} \{k_s[M(T), I(s)]\}(t)\, \mathrm{d}\mu(s) \cdot g(x)\right) \tag{14}$$

$$\frac{\partial T}{\partial t}(y,z,t) - k\left(\frac{\partial^2}{\partial y^2} + \frac{\partial^2}{\partial z^2}\right) T(y,z,t) = ku(t) \tag{15}$$

where $g(x)$ is a shear lag shape function[4] that determines the shear stress distribution along the embedded SMA, ρ is the density, EI is the flexural stiffness, c_D is the modulus of proportional damping, k is the thermal conductivity, and $u(t)$ is the square of the current applied to the SMA layer. The effective temperature at the SMA layer is determined via the mean value operator

$$[M(T)](t) = \frac{1}{A_{\mathrm{SMA}}} \int_{A_{\mathrm{SMA}}} T(y,z,t)\, \mathrm{d}y\, \mathrm{d}z \tag{16}$$

where A_{SMA} is the area of a single SMA layer. The problem statement is completed by specifying the initial displacement and velocity profiles along the beam, the initial temperature distribution of the cross section of the beam, and the appropriate boundary conditions for the beam and heat equations.

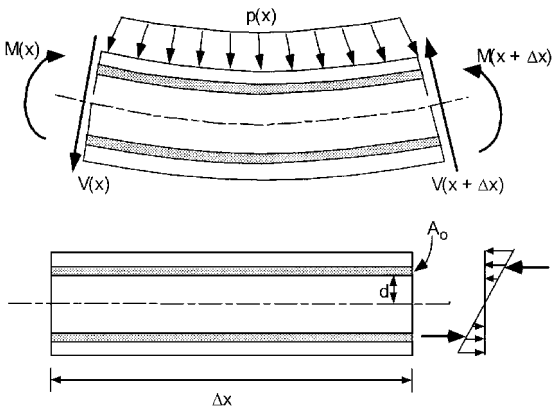

Fig. 3 Bernoulli–Euler beam with embedded SMA layers.

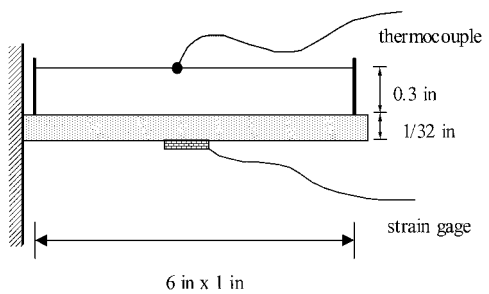

Fig. 4 Bernoulli–Euler beam with external SMA wire.

Example 3

Our third example is based on the SMA actuated beam shown in Fig. 4. The governing equations in this case can be expressed as

$$\rho\frac{\partial^2 w}{\partial t^2}+EI\frac{\partial^2}{\partial x^2}\left(\frac{\partial^2 w}{\partial x^2}\right)+c_D I\frac{\partial^2}{\partial x^2}\left(\frac{\partial^3 w}{\partial x^2\partial t}\right)$$

$$=\mathrm{d}\int_{\mathcal{S}_\Delta}\{k_s[M(T),I(s)]\}(t)\,\mathrm{d}\mu(s) \tag{17}$$

$$\frac{\partial T(y,z)}{\partial t}=\kappa\nabla^2 T+\frac{1}{\rho c}Q_0,\qquad y,z\in\Omega \tag{18}$$

$$k\frac{\partial T}{\partial n}=-h(T-T_\infty),\qquad y,z\in\partial\Omega \tag{19}$$

In Eq. (18), the quantities are as defined for example 1. As compared to example 2, he actuation wires are external in this case, so that the heat equation becomes simpler in form. In comparison to the last example, however, the heat equation in Eq. (18) is typically convection dominated, so that the time constant associated with cooling of the SMA wire determines the effective bandwidth of the actuator.

Example 4

As our final example, we consider the proof-of-concept design for the trailing edge repositioning system depicted in Figs. 5 and 6. As the number and lineal density of actuation elements increase (in the limit to an actuation sheet), we can approximate the linearly elastic response of a transverse section by

$$\langle\ddot{u}(t),v(t)\rangle_{V^*\times V}+c_D a[\dot{u}(t),v(t)]+a[u(t),v(t)]$$

$$=\sum_{i=1}^{4}\langle\{B_i[M(T),I]\}(t),v\rangle_{V^*\times V} \tag{20}$$

$$\frac{\partial T(y,z)}{\partial t}=\kappa\nabla^2 T+\frac{1}{\rho c}Q_0,\qquad y,z\in\Omega \tag{21}$$

$$k\frac{\partial T}{\partial n}=-h(T-T_\infty),\qquad y,z\in\partial\Omega \tag{22}$$

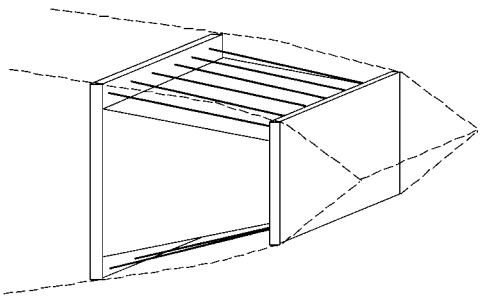

Fig. 5 Trailing-edge actuation: SMA repositioning design.

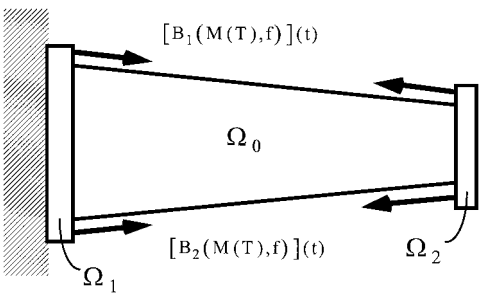

Fig. 6 Trailing-edge actuation: control of plane strain.

where

$$a(u,v)\equiv\int_\Omega\{2\mu\epsilon(u):\epsilon(v)+\lambda(\nabla\cdot u)(\nabla\cdot v)\}\,\mathrm{d}\Omega \tag{23}$$

$$V\equiv\left\{v\in H^1(\Omega):v|_{\Gamma_1}=0\right\} \tag{24}$$

$$\langle\{B_i[M(T),I]\}(t),v\rangle_{V^*\times V}=\{P_\mu[M(T),I]\}(t)\cdot\int_{\Gamma_i}g\cdot v\,\mathrm{d}s \tag{25}$$

In these equations, $u=(u,v)$ is the planar displacement field, $\epsilon(u)$ is the linear strain tensor, μ and λ are Lamé's constants, the quantities of Eq. (21) are as defined in example 1, and $H^1(\Omega)$ is the vector-valued Sobolev space defined as in Ref. 23.

IV. Identification Strategies

As we will see in Sec. V, the approach employed to develop control strategies for the systems defined in Eqs. (1–6) requires the construction of feedforward approximate inverses of the hysteretic control influence operator B_μ. The calculation of an approximate inverse $\hat{B}_\mu^{-1}$ for B_μ, in turn, requires that we obtain a reasonable approximation $\hat{B}_\mu$ of B_μ. Thus, the problem of identification is central to our control strategy. Although both on-line and off-line identification methods can be considered for the determination of $\hat{B}_\mu$, and subsequently $\hat{B}_\mu^{-1}$, we consider only off-line identification. Specifically, we assume that we are able to make structural measurements $\tilde{y}(t)$ that correspond to the observations $y(t;\mu)$ defined from the governing equations (1) and (2) as

$$y(t;\mu)=c_0 w(t;\mu)+c_1\dot{w}(t;\mu) \tag{26}$$

where c_0 and c_1 are appropriate (bounded) linear operators. The observations and solutions have been expressed as $y(t;\mu)$, $w(t;\mu)$, and $\dot{w}(t;\mu)$ to emphasize that they depend parametrically on the probability measure μ that characterizes the nonlinear, hysteretic control influence operator B_μ. We subsequently define the output error to be a functional of the probability measure $\mu(s)$ that defines a given rheological, integral hysteresis operator B_μ:

$$J(\mu)=\frac{1}{2}\int_0^T\|y(t;\mu)-\tilde{y}(t)\|_Z^2\,\mathrm{d}t$$

$$=\frac{1}{2}\int_0^T\left\{\|c_0 w(t;\mu)-\tilde{y}_0(t)\|_{Z_0}^2\right.$$

$$\left.+\|c_0\dot{w}(t;\mu)-\tilde{y}_1(t)\|_{Z_1}^2\right\}\mathrm{d}t \tag{27}$$

In general, this identification problem is difficult to solve because the dynamical system in Eqs. (1) and (2) evolves over an infinite-dimensional state space. Moreover, there is an infinite number of admissible probability measures over which we can search for the approximate, though optimal, control influence operator $\hat{B}_\mu$. A detailed discussion of the existence and uniqueness to the problem of identification of $\hat{B}_\mu$ is beyond the scope of this paper. The reader is referred to the discussion in Refs. 5 and 6 for a detailed discussion of the analysis in the case where there is no thermal evolution equation; for completeness, we summarize the spirit of the results.

Theorem 1: Consider the infinite-dimensional identification problem (ID) of finding $\mu^* \in \mathbb{M}_{ad}$ such that

$$J(\mu^*) = \inf_{\mu \in \mathbf{M}_{ad}} J(\mu)$$

where $J(\mu)$ is defined in Eq. (27), the observations $y(t; \mu)$ are defined in Eq. (26), and the structural response $w(t; \mu)$ and $\dot{w}(t; \mu)$ satisfy Eq. (1), where the temperature T in Eq. (1) is prescribed: 1) if B_μ is defined in terms of the Preisach kernel $\tilde{k}$ and we choose

$$\mathbb{M}_{ad} = \left\{ \mu : \mathrm{d}\mu = \sum_{i=1}^{N} \alpha_i g_i(s)\, \mathrm{d}s, \alpha_i \in [a, b] \right\}$$

where $a, b \in \mathbb{R}$ are fixed and N is fixed, or 2) if B_μ is defined in terms of the KP kernel $\hat{k}$ and we choose

$$\mathbb{M}_{ad} = \{\mu : \mu \text{ is a probability measure}\}$$

(including discrete measures), then there is a unique solution μ^* of the ID.

The distinguishing feature of cases 1 and 2 is that we must pose our optimization problem over a finite subspace of density functions for the Preisach operator. For the KP kernel, we can consider discrete probability measures in addition to those that are represented by density functions. Actual calculation of the optimal μ^* is not possible, in general, for case 2, inasmuch as it is selected from an infinite-dimensional space. We approximate μ^* from a finite set $\mathbb{M}_{ad,k} \subseteq \mathbb{M}_{ad}$, where $\mathbb{M}_{ad,k}$ is the set of all discrete probability measures having the form

$$\mu_k^* = \sum_{i=1}^{k} \mu_i \delta_{s_i} \tag{28}$$

Reference 6 shows that if we approximate the state $w(t)$ as in Eq. (3) and employ Eq. (28) to approximate the measure μ^*, we can pose a sequence of finite-dimensional identification problems (IDs).

Find $\mu_k^* \in \mathbb{M}_{ad,k}$ such that

$$J_N\left(\mu_k^*\right) = \inf_{\mu \in \mathbb{M}_{ad,k}} J_N(\mu) \tag{29}$$

where $J_n(\cdot)$ is the error functional associated with the N-dimensional Galerkin approximation of $J(\cdot)$ in Eq. (28) Under suitable approximation hypotheses,[6] we obtain a sequence of approximate solutions μ_k^* to the finite-dimensional IDs (29) that converge to the solution μ^* of Eq. (28):

$$\mu_k^* \to \mu$$

in distribution as $k, N \to \infty$.

V. Control Strategies

In this section, we derive control strategies for the cascade structure shown in Fig. 7, where the hysteretic operator B_μ is either 1) a Preisach operator or 2) a KP integral operator, as discussed in Sec. II. We employ the feedback control structure shown in Fig. 7. The primary components of the controller are the approximate hysteresis operator inverse $\hat{B}_\mu^{-1}$, approximate inverse G_0^{-1} for the heat equation, feedback controllers $K_1(s; \theta_1)$ and $K_2(s; \theta_2)$, and gains θ_0 and θ_4. In the following discussion, we assume that the feedback

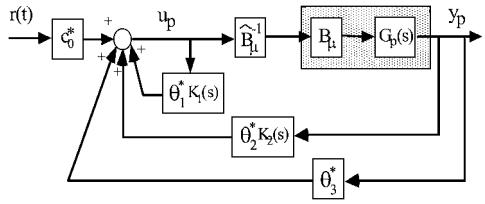

Fig. 7 Nonlinear control system: model reference control design.

controllers $K_1(s; \theta_1)$ and $K_2(s; \theta_2)$ have the frequency-domain representation

$$K_1(s; \theta_1) = \frac{N_k(s, \theta_1)}{D_k(s)} \tag{30}$$

$$K_2(s; \theta_2) = \frac{N_k(s, \theta_2)}{D_k(s)} \tag{31}$$

The following assumptions are standard for several variants of model reference control and model reference adaptive control for linear systems (see pp. 313–372 of Ref. 17 or Ref. 18).

1) The transfer function $G_0(s)$ characterizing the open-loop system has the form

$$G_0(s) = k_0 \frac{N_0(s)}{D_0(s)} \tag{32}$$

where $N_0(s)$ and $D_0(s)$ are monic polynomials and $N_0(s)$ is stable and of degree m_0.

2) The (upper bound for) degree n_0 of $D_0(s)$ is known.

3) The relative degree $\eta_0 = n_0 - m_0$ is known.

4) The sign of k_0 is known.

5) The transfer function $G_r(s)$ characterizing the reference model has the form

$$G_r(s) = k_r \frac{N_r(s)}{D_r(s)} \tag{33}$$

where $N_r(s)$ and $D_r(s)$ are stable, monic polynomials of degree m_r and n_r, respectively.

6) The relative degree $\eta_r = n_r - m_r$ of the reference model is equal to the relative degree of the open-loop transfer function $G_0(s)$.

If the nonlinear control influence operator is not present and we have a detailed knowledge of the plant $G_0(s)$ in Fig. 7, conventional model reference control techniques introduce the model matching condition (MMC) as follows:

The system depicted in Fig. 7 is said to satisfy the MMC provided that $c_0 = k_r/k_0$ and the gain θ_3 and the feedback controllers $K_1(s, \theta_1)$ and $K_2(s, \theta_2)$ satisfy

$$\begin{aligned} &N_k(s; \theta_1) D_0(s) + k_0 [N_k(s; \theta_2) + \theta_3 D_k(s)] N_0(s) \\ &\quad = D_k(s) D_0(s) - N_0(s) \tilde{D}_k(s) D_m(s) \end{aligned} \tag{34}$$

Properties that guarantee that we can, indeed, construct feedback controllers $K_1(s, \theta_1)$ and $K_2(s, \theta_2)$ and θ_3 that satisfy the MMC condition are well-known. Suppose for the moment that we consider only the linear components of the controller structure shown in Fig. 7. When controllers are designed based on the feedback system shown in Fig. 7 that satisfy the MMC in Eq. (34), the closed-loop system (for $B_\mu \equiv \hat{B}_\mu^{-1} \equiv 0$!) matches the desired response of the reference model $G_r(s)$. If the source of hysteresis B_μ in our cascade-structured, nonlinear system has the form of one of the integral hysteresis operators discussed in Sec. II, similar conclusions can be drawn provided that $\hat{B}_\mu^{-1} = B_\mu^{-1}$.

Theorem 2: Consider the nonlinear control system shown in Fig. 7 and suppose that 1) assumptions 1–6 are satisfied, 2) the controllers $K_1(s; \theta_1)$ and $K_2(s; \theta_2)$ satisfy the MMC, 3) B_μ is either a Preisach operator or a KP integral operator, and 4) $\hat{B}_\mu^{-1}$ is exactly equal to B_μ^{-1}.

Then 1) the closed loop system $G_c(s)$ is stable and 2) the response $y(t)$ tracks the reference model, i.e.,

$$\hat{y} = G_r(s) r \tag{35}$$

Proof: The proof of this theorem is immediate using the approach discussed in Ref. 2. All of the arguments remain unchanged when we employ the more general hysteresis operators discussed in this paper, instead of the piecewise linear hysteresis models presented in Ref. 2. The only detail left to consider is whether the Preisach and KP operators are, in fact, invertible. This nontrivial question is addressed at length several works.[12,14,15] For the class of Preisach operators and KP integral operators presented in Sec. II, both operators are invertible. □

When we utilize an output least squares identification theory, as discussed in detail in Refs. 5 and 6, the chances of realizing $\hat{B}_\mu^{-1} = B_\mu^{-1}$ in practice are remote, if not impossible. If we define the integral hysteresis identification error to be

$$e(t) = \left| \left[B_\mu^{-1}(u, I) \right](t) - \left[\hat{B}_\mu^{-1}(u, I) \right](t) \right| \tag{36}$$

we can interpret the nonlinear model error $e(t)$ as a disturbance to the linear control system. We have the following theorem guaranteeing the fidelity of the model reference control design methodology to identification error.

Theorem 3: Consider the nonlinear control system shown in Fig. 7 and suppose that 1) assumptions 1–6 are satisfied, 2) the controllers $K_1(s; \theta_1)$ and $K_2(s; \theta_2)$ satisfy the MMC, and 3) B_μ is either a Preisach operator or a KP integral hysteresis operator.

If we define the error in identification to be

$$e(t) = \left| \left[B_\mu^{-1}(u, I) \right](t) - \left[\hat{B}_\mu^{-1}(u, I) \right](t) \right| \tag{37}$$

the tracking error satisfies

$$\lim_{t \to \infty} \sup_{\tau > t} |y(\tau) - y_r(\tau)| \leq c \sup_{t \in [0, T]} |e(t)| \tag{38}$$

Proof: This theorem is a direct application of theorem (9.3.1) of Ioannou and Sun (Ref. 17, p. 652) or of corollary (4.1) of Tao and Kokotovic (Ref. 2, p. 70) for the choice of Preisach or KP integral hysteresis operator. □

Now consider the case when there is identification error in the hysteresis inverse model, which injects a disturbance into the system, and there is also modeling uncertainty in the plant. The authors are not aware of a general statement of stability that can be made in this case; however, for certain types of model uncertainty and using a conventional robust MRAC control scheme,[17] the following theorem ensuring boundedness can be made.

Theorem 4: Consider the nonlinear control system shown in Fig. 7. If the actual transfer function is given by

$$y_p = G_0(s)[1 + \Delta_m(s)](u_p + e) \tag{39}$$

where $G_0(s) = k_p[Z_p(s)/R_p(s)]$. Suppose that 1) assumptions 1–6 are satisfied, 2) B_μ is either a Preisach operator or a KP integral hysteresis operator, 3) e is a bounded disturbance given by the identification error of Eq. (36), 4) $\Delta_m(s)$, the multiplicative uncertainty, is analytic in $Re[s] \geq (-\delta_0/2)$ for some $\delta_0 > 0$, and 5) there exists a strictly proper transfer function $W(s)$ analytic in $Re[s] \geq (-\delta_0/2)$ and such that $W(s)\Delta_m(s)$ is strictly proper.

For any of the robust MRAC schemes of Table 9.1 in Ref. 17 satisfying theorem 9.3.2 therein (pp. 677, 678), guarantees that all of the signals in the closed-loop plant are bounded.

VI. Numerical and Experimental Results

In this section, we provide results from a physcial experiment and a numerical simulation, which illustrate both the feedforward open-loop control using approximate inverses for hysteretic control influence operators, and the addition of MRC and MRAC schemes to close the loop. The physical experiment is used to investigate the implementation of a Preisach hysteresis model identified from experimental data. The Preisach model is inverted to provide feedforward tracking control, in which there is no tracking error feedback. The numerical simulation is used to investigate the effect of an inexact hysteresis model on the model reference adaptive controller discussed in Sec. V.

Example: Physical Experiment of Preisach Hysteresis Model Inversion

The setup of the physical experiment is shown in Fig. 4 and is represented mathematically by example 3 in Sec. III. The beam is aluminum with a cross section of $1 \times \frac{1}{16}$ in. The SMA wire is attached to two vertical posts, which are secured to the beam and constrained to remain perpendicular to the beam surface at the base. The distance between the posts is 6 in., and the wire is offset 0.25 in. from the neutral bending axis. The wire is a nickel–titanium alloy SMA, with a cross section of 0.027 in. The wire was given an initial prestrain of 6% before being attached to the undeformed beam. When the SMA is actuated thermally, the wire recovers its prestrain, exerting a bending moment on the beam proportional to the offset distance from the neutral axis. A K-type thermocouple placed directly on the wire provides temperature measurements of the SMA, while a strain gauge on the underside of the beam provides measurements of the surface strain.

The Preisach hysteresis model was identified from experimental data. The identified hysteresis model represents the coupled SMA wire nonlinearity and the static deflection equation for the Bernouli–Euler beam. It maps the SMA wire temperature T directly into beam surface strain γ, which is indicative of the shape of the beam. To implement an open-loop control scheme for tracking a reference beam strain signal, the inverse Preisach model maps the strain reference signal $\gamma_d(t)$ into a temperature reference signal $T_d(t)$, which would make the system follow the reference signal if the identified hysteresis model matched the actual system exactly. However, when heating the wire resistively, the quantity that we can control is not the temperature; it is the heat input into the wire via an applied current. To this end, we look at a simplified model of the heat equation (21) of example 3.

We can simplify the SMA wire as a point heat source at each element Δx along the wire length. The quantity of heat Q in an element of mass m is given by

$$Q = cmT = c\rho A \Delta x T, \qquad Q/\Delta x = c\rho_L T$$

If Q_t is the rate of heat flow through the element, and heat enters at the rate of Q_0 and leaves at a rate given by the convective term $h(T - T_\infty)$, then Q_t is given by

$$Q_t = -h(T - T_\infty) + Q_0 \tag{40}$$

If the temperature is a function only of time (for a point source there would be no cross section), then $Q_t = \rho_L c \dot{T}$, which gives a simplified equation for the heat rate in an SMA wire as

$$\begin{aligned} \dot{T} &= -(h/\rho_l c)(T - T_\infty) + (1/\rho_L c) Q_0 \\ &= -a(T - T_\infty) + bu \end{aligned} \tag{41}$$

where $a = h/\rho_l c$, $b = (r/A)(1/\rho_L c)$ from the definition of Q_0 of example 1 and $u = i^2$. By letting $\bar{T} = T - T_\infty$ and $\dot{\bar{T}} = \dot{T}$ due to $T_\infty \equiv$ const, Eq. (41) becomes an equation of a classical form for MRC, namely,

$$\dot{\bar{T}} = -a\bar{T} + bu \tag{42}$$

For a plant model of the form of Eq. (42), Ref. 17 (pp. 379–384) outlines a control strategy to make $\bar{T}$ track a reference signal $r(t)$,

$$u = -k^* \bar{T} + L^* \bar{T}_r \tag{43}$$

where $k^* = (a + a_m)/b$, $L^* = b_m/b$, and a_m and b_m are the reference model parameters. The exact values for the elements comprising a and b are not known; hence, they could not be computed. However, by using estimates of L^*, k^*, $L(t)$, and $k(t)$ and sending a sufficiently rich temperature signal for the SMA wire to track (off-line from the experimental setup), the estimates L and k were identified. The control diagram for this experiment is shown in Fig. 8, and it can be seen that the controller is closed loop for temperature control, but open loop for shape (beam strain) tracking.

Results for two different reference signals to track are shown in Figs. 9 and 10. Figure 9 shows the results of open-loop tracking of

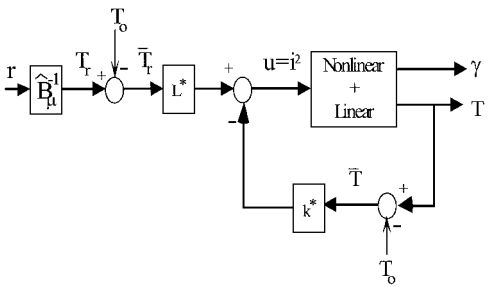

Fig. 8 Nonlinear temperature MRC design.

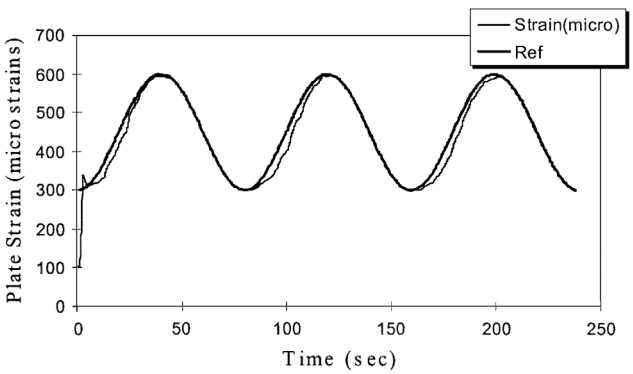

Fig. 9 Feedforward control of beam: Preisach hysteresis model.

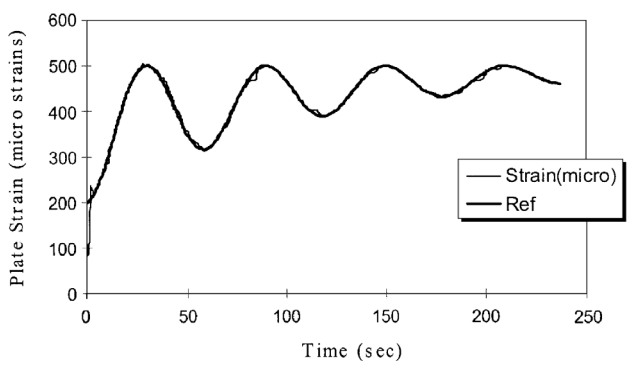

Fig. 10 Feedforward control of beam: Preisach hysteresis model.

a reference beam strain signal, whereas the latter shows the results with a simple proportional–integral (PI) strain feedback controller. The dynamics of the heat equation places a limit on how well the system can track a reference signal in that the cooling rate of the wire (and, hence, the decrease of beam strain) is limited by the convection with the air at room temperature. Despite the rough appearance of the tracking response, the results are excellent considering the thermocouple is calibrated to $\pm 2^\circ$C of precision.

Example: Numerical Simulation of Model Reference Control with Inverse Hysteresis Compensation

Because of the current limitations on the bandwidth of SMA actuators, we provide a numerical simulation in which we assume that the SMA actuator can achieve a high enough bandwidth to excite the dynamics of the system. We feel that this example provides an important conceptual bridge to the treatment of other, higher-bandwidth active materials such as MRF. Example 1 from Sec. III outlines the system equations of the SMA actuated mass-spring-damper system of Fig. 2. The hysteresis model used for this example is again of the Preisach type, but in this case it maps SMA wire temperature to force (via stress). The inverse model maps a desired force into temperature, which in this example is assumed to be directly controllable to eliminate the necessity for the temperature controller.

The controller structure is an MRAC structure (Fig. 7), with the parameters θ_1^*, θ_2^*, θ_3^*, and c_0^* considered to be unknown. There is a plethora of choices for adaptive laws for the model matching

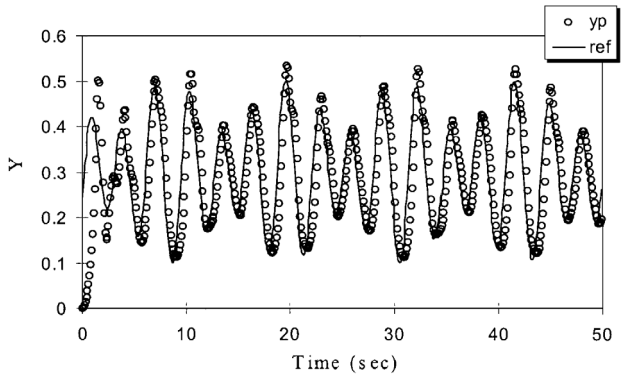

Fig. 11 MRAC of mass.

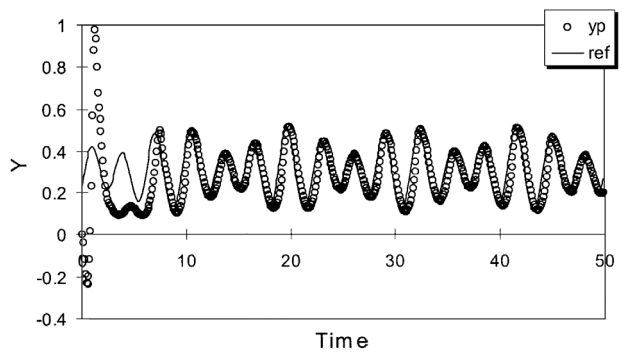

Fig. 12 MRAC of mass.

parameters[17]; the one used for this simulation can be found in Ref. 17 (pp. 359–360). For this MRAC scheme, if $\hat{B}_\mu^{-1} = B_\mu^{-1}$, i.e., there will be no disturbance injected into the system, then it is guaranteed that all signals in the closed-loop plant are bounded and the tracking error converges to zero asymptotically. If $r(t)$ is sufficiently rich, then the parameter error will converge to zero asymptotically. Two simulations were run, one in which $\hat{B}_\mu^{-1} = B_\mu^{-1}$ (Fig. 11) and one in which $\hat{B}_\mu^{-1}$ did not match exactly that of B_μ^{-1} (Fig. 12). It can be seen that for the case where the hysteresis inverse is an exact match to the actual model, the response locks on to the tracking signal very quickly. Even for the case with both unknown plant parameters and an inexact match for the approximate hysteresis inverse, Fig. 12 shows that the tracking error remains bounded. This fact suggests that, although there currently does not exist a proof of stability for this case, the adaptive control is well motivated and improves performance.

VII. Conclusions

We have presented a theory for treating classes of linear structural systems that are actuated by hysteretic active materials. By considering two types of integral hysteresis operator, we have derived existence and convergence of approximation methods for the problem of identifying the hysteretic control influence from structural measurements. Once we have identified the hysteretic control influence operator, we have derived MRC and MRAC methods based on an approximate feedforward compensator for the hysteresis. Numerical and experimental results have been given to validate the theory described herein. We note that, although the identification results presented hold for (possibly) infinite-dimensional dynamical systems, the closed-loop control designs assume finite-dimensional dynamical systems. The authors are currently investigating the extension of the closed-loop results to consider this class of systems.

References

[1]Hughes, D., and Wen, J., "Preisach Modeling of Piezoceramic Hysteresis; Independent Stress Effect," *Smart Structure and Materials 1995: Mathematics and Control in Smart Structures*, edited by V. V. Varadan, Springer–Verleg, Berlin, 1995, pp. 328–336.

[2]Tao, G., and Kokotovic, P., *Adaptive Control of Systems with Actuator and Sensor Nonlinearities*, Wiley, New York, 1996, pp. 53–90, 147–156.

[3]Kamath, G., Hurt, M., and Wereley, N., "Analysis and Testing of Bingham Plastic Behavior in Semi-Active Electrorheological Fluid Dampers," *Smart Material Structures*, Vol. 5, No. 4, 1996, pp. 576–590.

[4]Lagoudas, D., Bo, Z., and Qidwai, M., "A Unified Thermodynamic Constitutive Model for SMA and Finite Element Analysis of Active Metal Matrix Composites," *Mechanics of Composite Structures*, Vol. 3, No. 2, 1996, pp. 153–179.

[5]Banks, H., Kurdila, A., and Webb, G., "Identification of Hysteretic Control Influence Operators Representing Smart Actuators, Part (i): Formulation," *Journal of Mathematical Problems in Engineering* (submitted for publication).

[6]Banks, H., Kurdila, A., and Webb, G., "Identification of Hysteretic Control Influence Operators Representing Smart Actuators, Part (ii): Convergent Approximations," *Journal of Mathematical Problems in Engineering* (submitted for publication).

[7]Tanaka, K., Nishimura, F., and Tobushi, H., "Transformation Start Lines in Tini and Fe-Based Shape Memory Alloys After Incomplete Transformations Induced by Mechanical and/or Thermal Loads," *Mechanics of Materials*, Vol. 19, No. 2, 1991, pp. 271–280.

[8]Liang, C., and Rogers, C., "The Multi-Dimensional Consitutive Relations of Shape Memory Alloys," AIAA Paper 91-1165, Nov. 1991.

[9]Ivshin, Y., and Pence, T., "Constitutive Model for Hysteretic Phase Transition Behaviour," *International Journal of Engineering Science*, Vol. 32, No. 4, 1994, pp. 681–704.

[10]Coleman, B., and Hodgon, M., "A Constitutive Relation for Rate-Independent Hysteresis in Ferromagnetically Soft Materials," *International Journal of Engineering Science*, Vol. 24, No. 6, 1986, pp. 897–919.

[11]Coleman, B., and Hodgon, M., "On a Class of Constitutive Relations for Ferromagnetic Hysteresis," *Archives for Rational Mechanics and Analysis*, Vol. 99, No. 4, 1987, pp. 375–396.

[12]Krasnoselskii, M., and Pokrovskii, A., *Systems with Hysteresis*, Nauka, Moscow, 1983, pp. 6–20.

[13]Mayergoyz, I., *Mathematical Models of Hysteresis*, Springer–Verlag, Berlin, 1991, pp. 1–63.

[14]Visintin, A., *Differential Models of Hysteresis*, Springer–Verlag, Berlin, 1994, pp. 59–96.

[15]Brokate, M., "Hysteresis Operators," *Phase Transitions and Hysteresis*, edited by A. Visintin, Vol. 1584, Lecture Notes in Mathematics, Springer–Verlag, Berlin, 1994, pp. 1–38.

[16]Macki, J., Nistri, P., and Zecca, P., "Mathematical Models for Hysteresis," *SIAM Review*, Vol. 35, No. 1, 1993, pp. 94–123.

[17]Ioannou, P., and Sun, J., *Robust Adaptive Control*, Prentice–Hall, Englewood Cliffs, NJ, 1996, pp. 313–372, 375–384, 652, 677, 678.

[18]Sastry, S., and Bodson, M., *Adaptive Control*, Prentice–Hall, Englewood Cliffs, NJ, 1989, pp. 30–86.

[19]Tao, G., and Kokotovic, P., "Adaptive Control of Plants with Unknown Hysteresis," *IEEE Transactions on Automatic Control*, Vol. 40, No. 2, 1995, pp. 200–212.

[20]Ditman, J., Bergman, L., and Tsao, T.-C., "The Design of Extended Bandwidth Shape Memory Alloy Actuators," AIAA Paper 94-1757, April 1994.

[21]Baz, A., Imam, K., and McCoy, J., "Active Vibration Control of Flexible Beams Using Shape Memory Actuators," *Journal of Sound and Vibration*, Vol. 140, No. 4, 1991, pp. 437–456.

[22]Banks, H., Smith, R., and Wang, Y., *Smart Material Structures Modeling, Estimation and Control*, Wiley, New York, 1996, pp. 99–113.

[23]Brenner, S., and Scott, L., *The Mathematical Theory of Finite Element Methods*, Springer–Verlag, New York, 1994, pp. 215–225.